https://doi.org/10.5194/wes-2020-83
Preprint. Discussion started: 9 July 2020

eawe european academy of wind energy
Open Access WIND ENERGY SCIENCE DISCUSSIONS

Wind inflow observation from load harmonics: initial steps towards a field validation

Marta Bertelè[1], Carlo L. Bottasso[1], and Johannes Schreiber[1]
[1]Wind Energy Institute, Technische Universität München, Garching bei München, D-85748 Germany
Correspondence to: C.L. Bottasso (carlo.bottasso@tum.de)

Abstract.

A previously published wind sensing method is applied to an experimental dataset obtained on a 3.5 MW turbine and a nearby hub-tall met-mast. The method uses blade load harmonics to estimate rotor-equivalent shears and wind directions at the rotor disk. A second independent method is used to extend the met-mast-measured shear above hub height to cover the entire rotor disk.

Although the experimental setup falls short of providing a real validation of the method, it still allows for a realistic practical demonstration of some of its main features. The method appears to be robust to turbulent fluctuations and air density changes. Results indicate a good quality of the estimated shear, both in terms of 10-min averages and of resolved time histories, and a reasonable accuracy in the estimation of the yaw misalignment.

1 Introduction

This paper presents a first attempt at the field validation of a wind sensing method based on load harmonics.

Wind sensing refers to the general concept of using the response of the turbine to estimate characteristics of the inflow, which can be done in several different ways (Bottasso et al., 2010; Bottasso and Riboldi, 2014; Simley and Pao, 2016; Bottasso and Riboldi, 2015; Bertelè et al., 2017; Bottasso et al., 2018; Schreiber et al., 2020). Information on the inflow can support a variety of applications, including turbine and farm-level control, lifetime assessment and fatigue consumption estimation, power and wind forecasting, and others (Schreiber et al., 2020). In wind sensing, the rotor response is typically measured in the form of blade loads. If blade load sensors are already available, for example for load-mitigating control, wind sensing is a way of augmenting the value of load sensors, by providing an extra set of uses to the data that they already collect.

The method based on load harmonics was first proposed by Bottasso and Riboldi (2014), and then further elaborated and improved by Bottasso and Riboldi (2015); Cacciola et al. (2016a); Bertelè et al. (2017, 2018, 2019). In a nutshell, this method is based on the fact that some characteristics of the inflow (horizontal and vertical shear, lateral and vertical misalignment angles) generate a specific response of the rotor at the 1P (once per revolution) frequency. This is a very desirable feature, because:

- The 1P frequency is strongly dominated by these "deterministic" characteristics of the wind, and much less so by turbulent fluctuations (Bertelè et al., 2017);

https://doi.org/10.5194/wes-2020-83
Preprint. Discussion started: 9 July 2020

eawe european academy of wind energy
Open Access WIND ENERGY SCIENCE DISCUSSIONS

- Low frequencies are easier to measure than higher frequencies, as they require slower sampling rates (typically around one second for capturing the 1P of a wind turbine);
- There should be limited variability in such low frequencies among different installations of a same wind turbine type;
- The lower spectrum of the response of a wind turbine should be reasonably well captured by existing simulation tools used for design and certification.

The load-harmonic method requires a training dataset consisting of measured rotor loads and corresponding measured wind characteristics. The dataset can be based on experimental measurements, or be generated synthetically using a simulation model; these two approaches were respectively termed model-free and model-based in Bottasso and Riboldi (2014). Here we consider the former approach; indeed, a model might not always be available, for example in cases when wind sensing is applied to a turbine without the support of the manufacturer. Even when a model is available, it might not have been fully validated, so that a purely data-driven approach has a significant appeal. Thanks to the rotational symmetry of the rotor (Bertelè et al., 2019), the measured wind conditions that are necessary for training can be limited to the vertical shear and the horizontal (or yaw) misalignment; based on these quantities, the effects caused by horizontal shear and vertical (upflow) misalignment can be reconstructed. After training, the method can estimate the four wind parameters online during turbine operation simply from measured rotor loads.

It is envisioned that, in a practical application of the model-free harmonic-based method, the training phase would be a one-off activity performed at a test site equipped with a met-mast or other wind measuring devices such as lidars or sodars (Carswell, 1983; Vogt and Thomas, 1995; Lang and McKeogh, 2011). Indeed, hub-tall met-masts are routinely used during certification (IEC, 2017), and could be employed for the additional purpose of training the observer. After training, the method could be used on other installations of that same turbine type at normal production sites without necessitating of met-masts or other devices.

Goal of this paper is to present the application of the load-harmonic estimator to field test data collected at a test site on a 3.5 MW wind turbine and a nearby met-mast (Schreiber et al., 2020; Bertelè and Bottasso, 2020). This experimental setup is a realistic representation of the scenario outlined above, where a hub-tall met-mast is located in close proximity of a wind turbine for certification purposes. From this point of view, the present dataset provides opportunities not only for a first —partial— field demonstration of the method, but also for addressing some important practical implementational aspects.

Specifically, the vertical shear requires special attention. In fact, a hub-tall met-mast with more than one anemometer can only measure the wind shear over the lower part of the rotor disk; on the other hand, the load-harmonic observer estimates a rotor-equivalent shear (i.e. a shear over the entire rotor disk area). For large modern rotors, half-rotor or full-rotor shears are not necessarily equal (Murphy et al., 2019; Schreiber et al., 2020). Therefore, a way is needed to extend the measurement of the inflow above the met-mast, possibly without resorting to extra wind-scanning equipment to reduce cost and complexity. This problem is solved here using yet another wind sensing method (Bottasso et al., 2018; Schreiber et al., 2016, 2020). This second approach uses blade loads to estimate the average local speed over sectors of the rotor disk; from these sector-equivalent wind speeds, one can then estimate shears, including a vertical shear defined over just the lower half of the rotor.

https://doi.org/10.5194/wes-2020-83
Preprint. Discussion started: 9 July 2020

The sector-effective speed and load-harmonic observers have distinct characteristics, which make them somewhat complementary and applicable to different scenarios. In fact, the sector-effective observer does not need to be trained with data before it can be used, which is particularly useful in the case considered here, but can only reconstruct shears and not wind directions (Schreiber et al., 2020). On the contrary, the load-harmonic observer can reconstruct both shears and directions but needs to be trained from data, which is a potential complication. A three-step procedure is developed and demonstrated here, where the two observers are used in synergy:

1. The lower-half-rotor shear measured by the sector-equivalent speed method is tuned and validated with respect to the met-mast reference;

2. The full-rotor shear is computed using the validated sector-equivalent speed method, extending the measurement of the inflow above the met-mast;

3. This rotor-equivalent shear is finally used for training the harmonic-based estimator.

Although the present setup allows for a first demonstration of this procedure, it also presents some limitations that hinder a real and complete validation of the method. First, the extension of the shear above the met-mast is performed through the same rotor loads that are also used by the harmonic-based estimator. Clearly, a completely independent measurement of the inflow up to the tip of the rotor would be preferable for validation purposes. Second, the present met-mast only includes a wind vane at hub height. This is a point-wise measurement, whereas the one provided by the observer —being obtained through the response of the rotor— is a rotor-effective quantity. Here again, it would be desirable to train and verify the method with an independently-derived rotor-equivalent quantity. Third, a met-mast cannot really provide a true and absolute ground truth, as it measures the flow away from the rotor disk (two and half diameters away, in the present case). When the wind is not directly aligned with turbine and mast, the wind shear and direction may be slightly different, on account of wind spatial variability, orographic and vegetation-induced effects. These differences are indeed visible to some extent in the present dataset. Even when wind, mast and turbine are aligned, the two measurements are not co-located and therefore not necessarily identical. Clearly, a more precise characterization of the effective inflow experienced by the rotor disk would be desirable for validation purposes.

Although the present study clearly falls short of a true validation of the harmonic-based formulation of wind sensing, it still provides for an interesting and —in the authors' opinion— very promising insight into some of its characteristics.

The paper is organized as follows. Section 2 describes the overall methodology, including a brief review of the harmonic-based estimator in §2.2 and a description of the test site and the measurement of the inflow characteristics in §2.3. The analysis of the wind observer performance is presented in Section 3, while Section 4 concludes the paper.

https://doi.org/10.5194/wes-2020-83
Preprint. Discussion started: 9 July 2020

eawe european academy of wind energy
Open Access WIND ENERGY SCIENCE DISCUSSIONS

2 Methods

2.1 Wind parametrization

The wind inflow is described by four parameters: the vertical linear shear κ_v, the horizontal linear shear κ_h, the vertical wind misalignment angle (or upflow) χ, and the horizontal (or yaw) misalignment angle ϕ. These quantities are illustrated in Fig. 1.

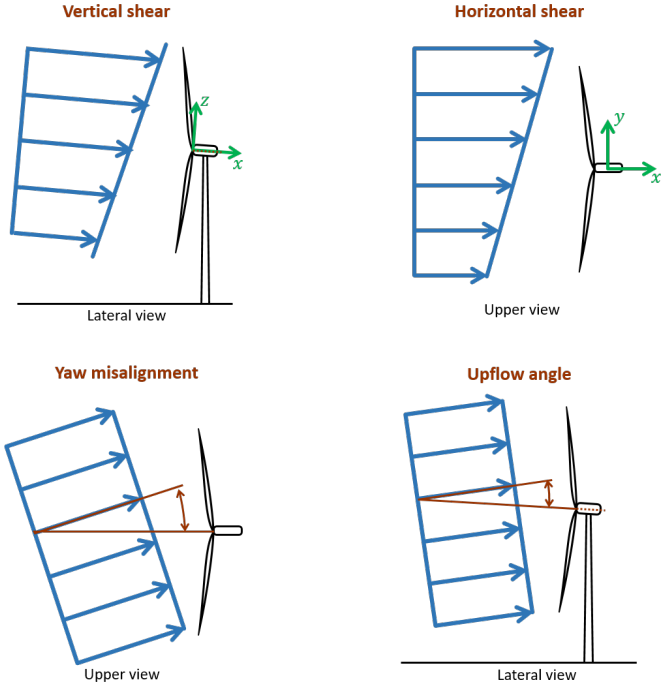

Figure 1. Definition of the four wind states used for parameterizing the wind field over the rotor disk.

A linearly sheared wind speed W at the rotor disk is defined as

$$W(y,z) = V_h \left(1 + \frac{y}{R}\kappa_h + \frac{z}{R}\kappa_v\right), \tag{1}$$

where V_h is the hub-height speed, and R the rotor radius. With reference to Fig. 1, the wind velocity vector components u, v and w along the x, y and z axes, respectively, of a hub-centered nacelle-attached frame write

$$u(y,z) = W(y,z)\sqrt{1-\tilde{v}^2-\tilde{w}^2}, \tag{2a}$$

$$v(y,z) = W(y,z)\tilde{v}, \tag{2b}$$

$$w(y,z) = W(y,z)\tilde{w}, \tag{2c}$$

https://doi.org/10.5194/wes-2020-83
Preprint. Discussion started: 9 July 2020

eawe european academy of wind energy
Open Access WIND ENERGY SCIENCE DISCUSSIONS

where $\tilde{v}$ and $\tilde{w}$ are defined as

$$\tilde{v} = \frac{v(0,0)}{V_h} = \sin\phi\cos\chi, \tag{3a}$$

$$\tilde{w} = \frac{w(0,0)}{V_h} = \sin\chi. \tag{3b}$$

For notational simplicity, the four wind parameters are grouped together in the wind state vector $\boldsymbol{\theta} = \{\tilde{v},\ \kappa_v,\ \tilde{w}, \kappa_h\}^T$. Given $\boldsymbol{\theta}$, the misalignment angles can be readily computed by inverting Eqs. (3) to get $\chi = \arcsin\tilde{w}$ and $\phi = \arcsin\tilde{v}/\cos\chi$.

2.2 Wind observer formulation

The relationship between wind states and rotor loads is assumed in the form

$$\boldsymbol{m} = \boldsymbol{F}(V,\rho)\boldsymbol{\theta} + \boldsymbol{m}_0(V,\rho) = [\boldsymbol{F}(V,\rho)\ \boldsymbol{m}_0(V,\rho)] \begin{bmatrix} \boldsymbol{\theta} \\ 1 \end{bmatrix} = \boldsymbol{T}\,\overline{\boldsymbol{\theta}}, \tag{4}$$

where $\boldsymbol{F}$ and $\boldsymbol{m}_0$ are model coefficients that depend on wind speed V and air density ρ. The dependency on wind speed is taken into account by discretizing the wind speed range in nodal values and linearly interpolating the model based on the current wind speed, while density is accounted for as explained in §2.2.1. The load vector $\boldsymbol{m}$ is defined as

$$\boldsymbol{m} = \left\{m_{1\mathrm{c}}^{\mathrm{OP}},\ m_{1\mathrm{s}}^{\mathrm{OP}},\ m_{1\mathrm{c}}^{\mathrm{IP}},\ m_{1\mathrm{s}}^{\mathrm{IP}}\right\}^T, \tag{5}$$

where m indicates the blade bending moment, subscripts $(\cdot)_{1\mathrm{s}}$ and $(\cdot)_{1\mathrm{c}}$ respectively indicate 1P sine and cosine harmonic amplitudes, while superscripts $(\cdot)^{\mathrm{OP}}$ and $(\cdot)^{\mathrm{IP}}$ indicate out- and in-plane load components, respectively. Harmonic components are obtained from measured blade loads using the Coleman transformation (Coleman and Feingold, 1958), followed by low pass filtering.

The model coefficients $\boldsymbol{F}$ are not all independent, because of the rotational symmetry of the rotor (Bertelè et al., 2019). In a nutshell, the effects on loads caused by the horizontal shear are the same as the ones caused by the vertical shear after a rotation of $\pi/2$; the same holds true for the wind misalignment angles. This not only reduces the number of unknowns, but also eases the identification of the model. In fact, whereas vertical shear changes naturally over a significant range (for example, because of diurnal fluctuations), horizontal shear does not (except in waked conditions). Similarly, whereas yaw misalignment changes significantly in normal operation because of the inability of the yaw system to immediately and exactly track wind direction fluctuations, upflow changes little (except that for orographic wind-direction-dependent effects). Therefore, a complete model can be identified simply from variable vertical shear and horizontal misalignment, because the effects of the other two wind states are obtained by the symmetry of the coefficients.

The model coefficients $\boldsymbol{T}$ are identified by stacking side by side measured wind states $\boldsymbol{\theta}$ into a matrix $\boldsymbol{\Theta} = [\overline{\boldsymbol{\theta}}_1, \ldots, \overline{\boldsymbol{\theta}}_N]$, while the corresponding measured blade loads $\boldsymbol{m}$ are stacked into matrix $\boldsymbol{M} = [\boldsymbol{m}_1, \ldots, \boldsymbol{m}_N]$, obtaining

$$\boldsymbol{M} = \boldsymbol{T}\boldsymbol{\Theta}. \tag{6}$$

https://doi.org/10.5194/wes-2020-83
Preprint. Discussion started: 9 July 2020

eawe european academy of wind energy
Open Access WIND ENERGY SCIENCE DISCUSSIONS

The model coefficients are then computed by least squares as

$$\boldsymbol{T} = \boldsymbol{M}\boldsymbol{\Theta}^T(\boldsymbol{\Theta}\boldsymbol{\Theta}^T)^{-1}. \tag{7}$$

Given the model coefficients, the estimated wind states $\boldsymbol{\theta}_{\mathrm{E}}$ are computed online from the measured loads $\boldsymbol{m}_{\mathrm{M}}$ as

$$\boldsymbol{\theta}_{\mathrm{E}} = \left(\boldsymbol{F}^T\boldsymbol{Q}^{-1}\boldsymbol{F}\right)^{-1}\boldsymbol{F}^T\boldsymbol{Q}^{-1}(\boldsymbol{m}_{\mathrm{M}} - \boldsymbol{m}_0), \tag{8}$$

where $\boldsymbol{Q}$ is the co-variance weighting matrix.

2.2.1 Density correction

Aerodynamic loads can be written as

$$m_{\mathrm{A}} = qAC, \tag{9}$$

where $q = 1/2\rho V^2$ is the dynamic pressure, A the rotor disk area and C a non-dimensional coefficient. A correction for density can be simply obtained as

$$m_{\mathrm{A_{ref}}} = m_{\mathrm{A_i}}\frac{\rho_{\mathrm{ref}}}{\rho_i}, \tag{10}$$

where ρ_{ref} is a reference density, and ρ_i the density corresponding to measurement $m_{\mathrm{A_i}}$.

However, blade load sensors measure not only aerodynamic loads but also the effects of inertia and gravity, which do not depend on air density. Inertial loads for a rotor spinning at constant rotor speed do not generate 1P harmonics, and hence do not appear in Eq. (4). On the other hand, gravitational terms generate 1P loads represented by the non-homogeneous term $\boldsymbol{m}_0$ in that same equation. According to Bertelè et al. (2017), this term can be written as

$$\boldsymbol{m}_0 = qA\boldsymbol{C} + \boldsymbol{g}. \tag{11}$$

The first term is a gravity-induced load due to the rotor deformation caused by aerodynamic loads; for example, if the blade bends under the push of thrust, the resulting deformation generates a non-null moment arm for gravity with respect to the blade root where the load sensor is located, resulting in a 1P load. This term is proportional to dynamic pressure and can be corrected for density. The second term $\boldsymbol{g}$ accounts for in-plane and out-of-plane gravity-induced loads, the latter being caused by blade precone, prebend and rotor uptilt. This term does not depend on density, and hence it should be eliminated by the equations before a density correction can be applied. To this end, the model coefficients of Eq. (4) were identified for a very low wind speed, just above cut-in. Here the effects caused by $qA\boldsymbol{C}$ are negligible, and hence $\boldsymbol{g} \approx \boldsymbol{m}_0$. Having first identified the gravity term $\boldsymbol{g}$ and then having eliminated it from model (4), each measured load was finally corrected for density using Eq. (10).

2.3 Wind parametrization in the field

Before wind states can be estimated at run time from measured loads using Eq. (8), the model coefficients must be identified through the simultaneous measurements of wind states and associated loads using Eq. (7). This section presents a practical

https://doi.org/10.5194/wes-2020-83
Preprint. Discussion started: 9 July 2020

eawe european academy of wind energy
Open Access WIND ENERGY SCIENCE DISCUSSIONS

method to perform this task, based on the use of a standard IEC-compliant (IEC, 2017) hub-tall met-mast. A similar procedure could be used to identify the observer for a specific wind turbine type. Having obtained the model coefficients, one should be able to use the same observer for other installations of that same wind turbine type. Although there is yet no direct demonstration of this assertion, it seems reasonable to assume that wind turbines of the same model will have a similar 1P response to shears and misalignment angles. Additionally, Bottasso and Riboldi (2015) showed that the method is fairly robust to changes in some of the wind turbine parameters that may vary among different installations of a same wind turbine type, including changes in the stiffness of foundations, orographic effects, imbalance due to pitch misalignment, miscalibration of the load sensors and changes in airfoil lift and drag due to soiling/erosion.

2.3.1 Test site

Figure 2 shows a panoramic view of the test site (Bromm et al., 2018), which is located in Germany a few kilometers inland from the Baltic Sea and characterized by gentle hills, open fields and forests. Data was measured between October 19 and November 29, 2017 on a 3.5 MW eno114 turbine designed and produced by eno energy systems GmbH. The turbine (labelled WT1 in the figure) has a 92 m hub height and a rotor radius of 114.9 m.

A met-mast is situated at about 2.5 diameters (D) from the turbine. Wind direction was measured at a height above ground of 89.3 m with a Thies GmbH wind vane, while wind speed measurements were obtained with three cup anemometers produced from the same company and located at 89.3 m, 91.5 m and at the lower tip of the rotor (about 34 m).

A second turbine (labelled WT2) is also present on site, and its wake affects the met-mast and WT1 for easterly and south-easterly winds. Similarly, the wake of WT1 affects the met-mast for northern wind directions. All these conditions were discarded from the training dataset, in addition to all other situations when WT1 was not in a normal power production state. A forest of 15-20 m tall trees is located 300 m east of WT1; as only wind directions $\Gamma \in [180, 340]$ deg were considered in this work, this high roughness area was never in the inflow direction. On the other hand, the town of Brusow is located about 1 km to the west of the site, and its effects on the inflow are unknown. A test campaign conducted at the same site in the period July-November of the previous year revealed an almost equal distribution of unstable, neutral and stable conditions, as measured by an eddy covariance station (Bromm et al., 2018).

Synchronized turbine and blade load data was sampled at 10 Hz on WT1. Blades 1 and 3 were equipped with strain gages, installed in close proximity of the blade roots and measuring both flapwise and edgewise bending components. The load on blade 2 was computed as the mean of the measurements of blades 1 and 3, shifted by $\pm\pi/3$. In general, sensors deployed in the field cannot be assumed to be always exactly calibrated, and they may suffer from a variety of issues that affect the quality of the measurements that they provide. To address this problem, it is useful to devise simple and practical ways to correct the measurements, even when the root cause of the problem is unknown. Here, consistent mismatches between the long-term mean readings of the two blade load sensors were observed; this problem was eliminated by scaling the measurements as $\overline{m}_1(1+s) = \overline{m}_3(1-s)$, with $s = 0.0274$. Additionally, the azimuth signal was corrected to account for sensor bias and dynamic effects, as explained in Schreiber et al. (2020). The turbine on-board wind vane was not used here, because these

https://doi.org/10.5194/wes-2020-83
Preprint. Discussion started: 9 July 2020

eawe european academy of wind energy
Open Access WIND ENERGY SCIENCE DISCUSSIONS

sensors typically require a careful calibration to correct for nacelle and rotor effects. The yaw encoder signal was also corrected for an apparent inconsistency of its readings, as explained later in this section.

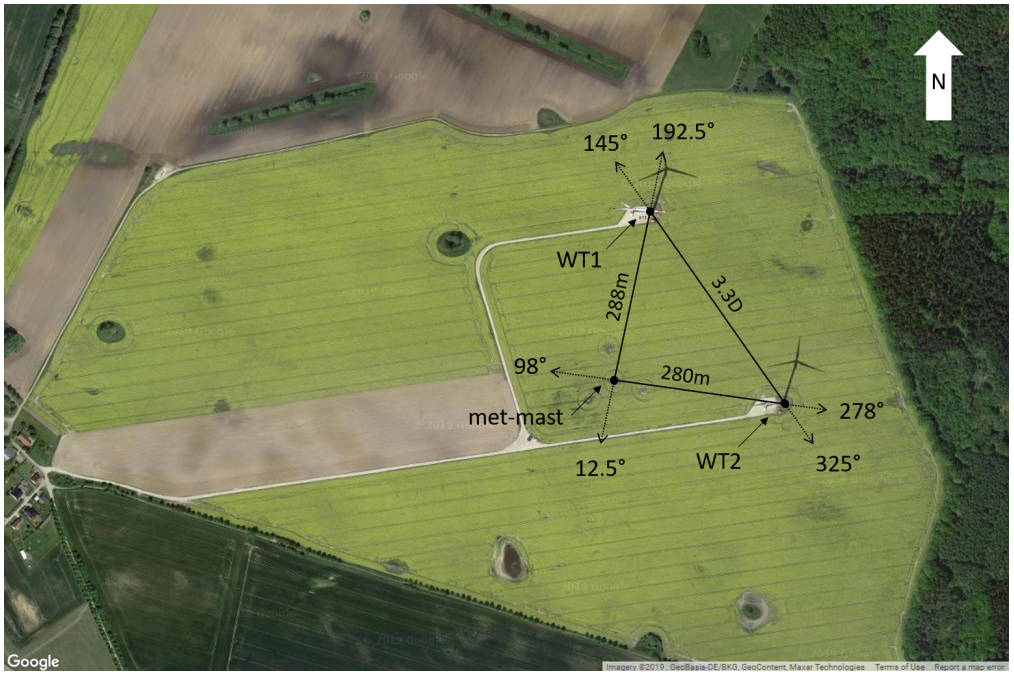

Figure 2. Satellite view of the test site, including waking directions and distances. WT1 indicates the turbine used for the present analysis (© Google Maps).

2.3.2 Wind shears

The met-mast present at the test site reaches only up to hub height; this is also the typical case of IEC-compliant met-masts used for certification (IEC, 2017). The three anemometers at 34, 89 and 92 m can be used to estimate the shear over the lower half of the rotor, which however in general differs from the shear computed over the whole rotor height.

To address this issue, the sector-effective wind speed (SEWS) estimation method described in Schreiber et al. (2020) was employed. In a nutshell, the blades are used as local speed sensors that, scanning the rotor disk, provide average speeds over four rotor quadrants. By using the two lateral and the lower quadrants, the shear over the lower part of the rotor disk can be computed. This quantity is validated with respect to the shear measured by the met-mast, assumed as a ground truth. Then, having verified a good correlation between the measured and estimated shears over the lower part of the rotor, the average speeds for all four quadrants are used to calculate the wind shear over the whole rotor disk. A brief overview of the SEWS estimator is reported next, and the interested reader is referred to Schreiber et al. (2020) for further details.

https://doi.org/10.5194/wes-2020-83
Preprint. Discussion started: 9 July 2020

eawe european academy of wind energy
Open Access WIND ENERGY SCIENCE DISCUSSIONS

The rotor cone coefficient is defined as

$$C_m\left(\beta,\lambda,q,\psi_i\right)=\frac{m_i}{0.5\rho A R V^2}, \tag{12}$$

where β is the pitch angle, $\lambda=\Omega R/V$ the tip speed ratio and Ω the rotor speed, m_i the out-of-plane bending load of the ith blade and ψ_i its azimuthal position. Coefficient C_m was computed here with the aeroelastic code FAST (Jonkman and Jonkman, 2018). Inverting Eq. (12), a look-up table (LUT) is generated that returns the blade-effective wind speed V_i given measured blade pitch angle, rotor speed, azimuthal blade position, bending moment and density:

$$V_i=\mathrm{LUT}_{C_m}\left(\beta,\Omega,\psi,m_i,\frac{\rho}{\rho_{\mathrm{ref}}}\right). \tag{13}$$

This way each individual blade is turned into a local wind speed sensor, which scans the rotor disk. Since this local measurement is noisy, the rotor disk is divided into sectors of area A_{S}, and a sector-equivalent wind speed is computed as

$$V_{\mathrm{S}}=\int_{A_{\mathrm{S}}} V_i(\psi_i)\,\mathrm{d}A_{\mathrm{S}}. \tag{14}$$

Here the four sectors shown in Fig. 3 were used. This yields four measurements of the local speed at the rotor disk, located at $2/3\,R$ above, below and to the sides of the hub center (Bottasso et al., 2018).

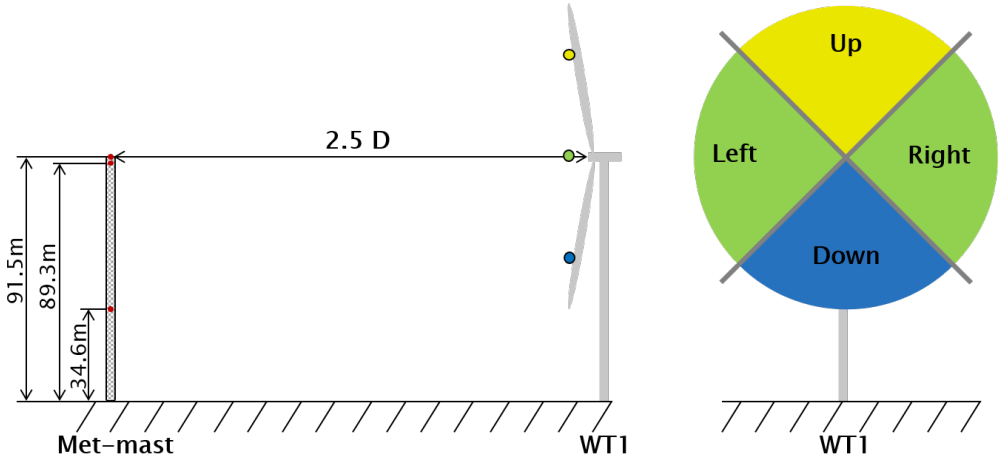

Figure 3. Definition of the four rotor sectors and their relative position with respect to the met-mast. Right: view looking downstream.

The rotor-effective horizontal linear shear can be computed inserting the sector-effective wind speeds in Eq. (1) to get

$$\kappa_h=\frac{3}{2}\frac{V_{\mathrm{S,left}}-V_{\mathrm{S,right}}}{V_{\mathrm{S,left}}+V_{\mathrm{S,right}}}. \tag{15}$$

For a more coherent comparison of the linear vertical shears estimated by the met-mast and by the sector-effective speeds, it is useful to first fit a power law to the respective wind speed measurements, as they are obtained at different heights above

https://doi.org/10.5194/wes-2020-83
Preprint. Discussion started: 9 July 2020

eawe european academy of wind energy
Open Access WIND ENERGY SCIENCE DISCUSSIONS

ground. The power law profile is defined as

$$V(z)_{\mathrm{PL}} = V_{\mathrm{ref}} \left(\frac{z+H}{H} \right)^{\alpha}, \tag{16}$$

where H is the height of the hub, V_{ref} the wind speed at that point, and α the power law exponent. Given n measurements V_i at z_i, the parameters of the power law are computed by the following best fit:

$$(V_{\mathrm{ref}}, \alpha) = \arg \min_{V_{\mathrm{ref}}, \alpha} \sum_{i=1}^{n} \left(V_{\mathrm{PL}}(z_i) - V_i \right)^2. \tag{17}$$

Notice that two measurements at two different heights are sufficient to estimate the power law. Having solved the fitting problem (17), the linear shear κ_v between heights z_A and z_B is computed as

$$\kappa_v = \frac{R(V_{\mathrm{PL}}(z_A) - V_{\mathrm{PL}}(z_B))}{z_A V_{\mathrm{PL}}(z_B) - z_B V_{\mathrm{PL}}(z_A)}. \tag{18}$$

The left plot of Fig. 4 shows the correlation between 10-min averages of the vertical shears obtained by the met-mast and by the sector-effective wind speeds on the lower half of the rotor. Only wind directions between 170 and 220 deg are considered, where the turbine and met-mast are aligned. The power law for the met-mast was obtained by using all three speed measurements, although the two at 89.3 and 91.5 m above ground are almost coincident. For the sector-effective estimator the power law was obtained by using the two measurements $(V_{\mathrm{S,left}} + V_{\mathrm{S,right}})/2$ at $z = 0$, and $V_{\mathrm{S,down}}$ at $z = -2/3\,R$. For both cases, the lower-half-rotor linear shear was computed from Eq. (18) using $z_A = 0$ and $z_B = -R$ and the corresponding fitted power law. The figure shows that there is a good correlation between the two lower-half-rotor shears, resulting in a Pearson's coefficient of 0.906. However, the figure also shows that the linear fit (red dashed line) has a different slope than the ideal match (black solid line). The results presented later in Section 3 were corrected to account for this error.

For the same data points, the right plot of Fig. 4 shows the correlation between the vertical shears obtained by the met-mast and by the sector-effective estimator over the complete rotor. Here again the power law for the met-mast was obtained by using all three speed measurements. For the sector-effective estimator the power law was obtained by using the three measurements $V_{\mathrm{S,up}}$ at $z = 2/3\,R$, $(V_{\mathrm{S,left}} + V_{\mathrm{S,right}})/2$ at $z = 0$, and $V_{\mathrm{S,down}}$ at $z = -2/3\,R$. For both cases, the full-rotor linear shear was computed from Eq. (18) using $z_A = R$ and $z_B = -R$ and the corresponding power laws. It should be noted that, since the height of the top anemometer reaches only up to hub height, for the met-mast the calculation of the full rotor shear implies a considerable extrapolation outside of the available measurements.

Comparison of the right and left plots of Fig. 4 shows that in the full-rotor case there is a lower correlation between the met-mast and the SEWS observer than in the lower-half rotor case. This indicates that the shear changes over the height of the rotor disk. In addition, as expected for a typical power law where the profile gradient increases with height, the lower-half-shear coefficient is typically higher than the full-rotor one.

Based on these results, it appears that the rotor-effective shear used for identifying the model of §2.2 would require a tall met-mast or other wind measurement devices such as lidars or sodars capable of scanning the inflow reaching the top of the rotor. Here —as such a tall mast was not available— an alternative approach was used: the sector-equivalent wind speed method was used to virtually extend the met-mast measurements to the required height. Based on the good correlation shown by the

https://doi.org/10.5194/wes-2020-83
Preprint. Discussion started: 9 July 2020

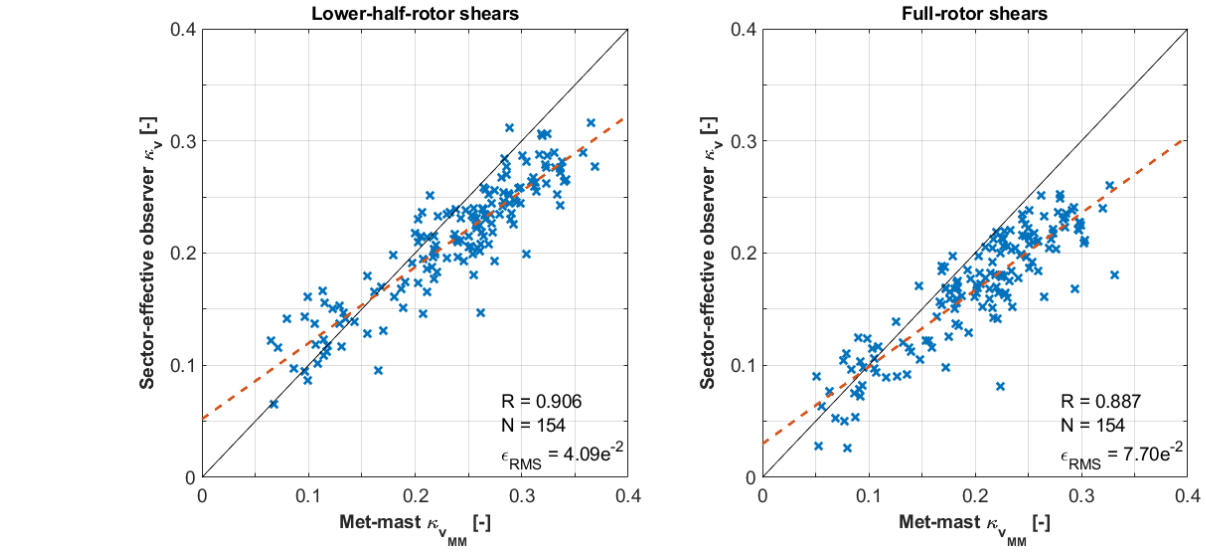

Figure 4. Correlation between 10-min averages of the vertical linear shears measured with the met-mast and the sector-effective observer. Left: lower-half rotor shears; right: full-rotor shears. Red dashed line: linear best fit; black dashed line: ideal match; R: Pearson's correlation coefficient; N: number of data points; ϵ_{RMS}: root mean square error.

left plot of Fig. 4 for the lower-half-rotor shear, it was concluded that the two lateral and the lower sector-equivalent speeds are sufficiently accurate for the purpose of estimating shears. Since the top sector speed is based on exactly the same calculation procedure as the other ones, all four speeds were then used to estimate the full-rotor shear, which in turn was used as reference for the identification of the model of §2.2.

Unfortunately a similar validation cannot be performed for the horizontal shear with the present met-mast, because of the lack of multiple lateral measurements. However, the horizontal shear is based on the same sector-equivalent wind speeds that estimate the vertical shear with good accuracy, so that there is no reason to believe that Eq. (15) should not provide a similarly good-quality estimate. Additionally, the horizontal shear based on the two lateral sector-effective wind speeds was shown in Schreiber et al. (2020) to track the movement of an impinging wake with remarkable accuracy.

2.3.3 Wind misalignment angles

The met-mast is equipped with a single wind vane measuring the wind direction Γ at hub height. Unfortunately, this means that only a point-wise measurement is available, instead of the rotor-equivalent one that would be ideally necessary for the training of the load-harmonic method of §2.2. This is a limit of the current setup and of the present attempt at validating the approach. Nonetheless, a pragmatic choice was made here to filter the wind vane signal with a moving average to remove the faster fluctuations, and to use this signal as a proxy for the rotor-effective horizontal wind direction. The misalignment angle between turbine and wind was obtained by subtracting the absolute yaw angle of the nacelle from the met-mast-measured

https://doi.org/10.5194/wes-2020-83
Preprint. Discussion started: 9 July 2020

eawe european academy of wind energy
Open Access WIND ENERGY SCIENCE DISCUSSIONS

wind direction. The result was shifted in time on account of the distance between turbine and met-mast, the time delay being computed from the average wind speed.

The top plot of Fig. 5 shows 10-min averages of the resulting met-mast yaw misalignment angle Φ_{MM}, plotted as a function of wind direction Γ. The clear trend visible in the plot is probably due to a miscalibration of the nacelle yaw encoder. Indeed, Bromm et al. (2018) also noticed a non-constant offset when comparing the turbine SCADA orientation with the one provided by a temporarily installed GPS system. This trend was removed using the first ten days of data, excluding waked directions, obtaining the bottom plot of Fig. 5.

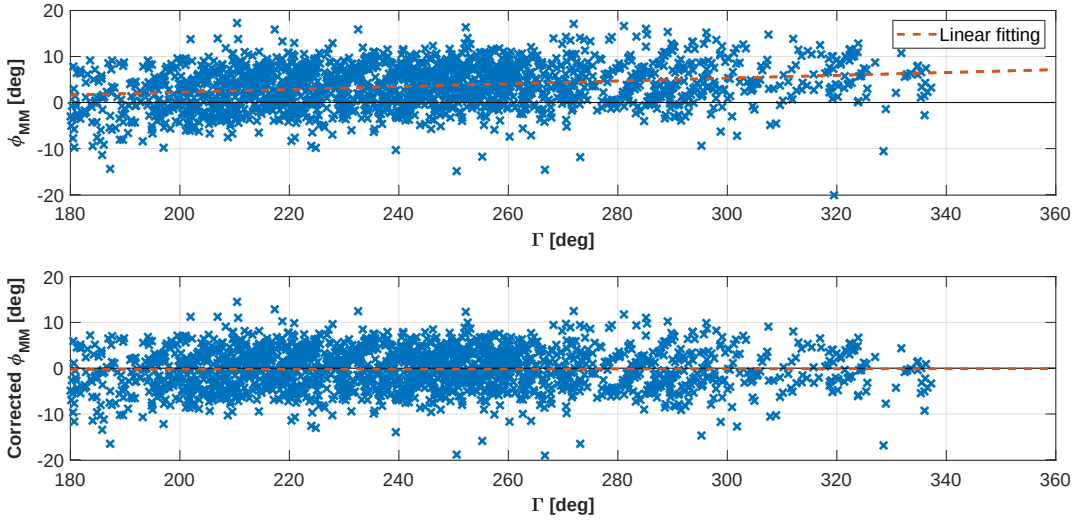

Figure 5. 10-min averages of met-mast horizontal wind misalignment angle ϕ_{MM} vs. wind direction at the met-mast Γ, before (top) and after (bottom) correction for yaw encoder error.

As the current setup does not provide for measurements of the upflow, the rotational symmetry of the rotor was used to compute the relevant model coefficients.

2.3.4 Wind speed and density

Since the load-wind model expressed by Eq. (4) depends on the operating conditions, a rotor-effective wind speed was computed with the torque balance equation (Ma et al., 1995; Van der Hooft and Engelen, 2004; Soltani et al., 2013; Schreiber et al., 2020) and used as scheduling parameter of the wind observer. Figure 6 shows an excellent correlation for the 10-min averages of the computed rotor-effective wind speed and the met-mast hub-height speed. Density was obtained from the ideal gas law based on temperature, since no additional information was available, and was used to rescale the load measurements.

https://doi.org/10.5194/wes-2020-83
Preprint. Discussion started: 9 July 2020

eawe european academy of wind energy
Open Access WIND ENERGY SCIENCE DISCUSSIONS

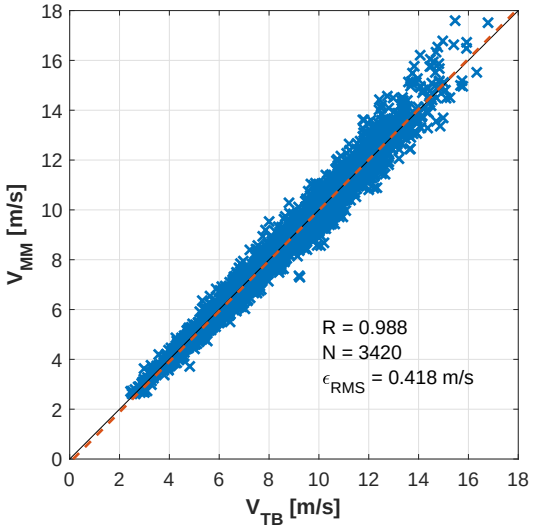

Figure 6. Correlation between 10-min averages of met-mast hub-height wind speed V_{MM} and rotor-effective wind speed V_{TB} estimated with the torque balance equation. Red dashed line: linear best fit; black dashed line: ideal match; R: Pearson's correlation coefficient; N: number of data points available; ϵ_{RMS}: root mean square error.

3 Results

3.1 Model identification

The observer coefficients were identified with Eq. (7) using the horizontal and vertical shears obtained from the sector-effective wind speeds, and the yaw misalignment angle computed from the met-mast wind vane and the nacelle yaw encoder, corrected according to Fig. 5. The upflow model coefficients were obtained from the rotational symmetry of the rotor behavior. The model coefficients were scheduled as functions of the rotor-effective wind speed computed from the torque balance equation, and load measurements were corrected for density.

The model was identified based on 10-min averages. The wind speed nodes of the linear parameter varying model (4) were defined as $V = [4,\ 5,\ 6.5,\ 8,\ 9,\ 10,\ 12,\ 13.5]$ m/s, while the reference density was set to 1.238 kg/m^3. Table 1 shows the range covered by each parameter within the training dataset.

About 15% of the available data was used for identification, leaving about 370 hours of measurements for validation. In the following, the performance of the harmonic observer is evaluated solely based on the validation dataset.

A similar identification was also performed using the same training set, but using instantaneous 10 Hz measurements instead of 10-min averages. As this led to a small decrease in model performance, it was concluded that some time averaging may be beneficial as it probably alleviates the effects of possible outliers.

https://doi.org/10.5194/wes-2020-83
Preprint. Discussion started: 9 July 2020

eawe european academy of wind energy
Open Access WIND ENERGY SCIENCE DISCUSSIONS

Table 1. Minimum and maximum values of rotor effective wind speed, turbulence intensity (TI), density, yaw misalignment, vertical and horizontal shear within the training dataset.

	V [m/s]	TI [%]	ρ [kg/m^3]	ϕ_{MM} [deg]	κ_v [-]	κ_h [-]
min	3.89	1.15	1.221	-12.66	-0.045	-0.053
max	13.68	11.06	1.256	8.28	0.242	0.087

3.2 Wind observer performance

Figure 7 gives an overview of the model performance in terms of correlations between 10-min averages of reference and observed parameters, using the validation sub-set for wind speeds above 8 m/s. For each parameter, one per subplot, the reference state is shown on the x axis, whereas the observed one on the y axis. For the shears, the Pearson's correlation coefficients (R) is above 0.9, and the root mean square (RMS) error ϵ_{RMS} is of the order of 10^{-3}. The yaw misalignment angle is less accurate, possibly because the reference is point-wise whereas the estimate is rotor-effective. Indeed, investigations at the same site with a more complete setup including a lidar profiler reported significant veer at the inflow (Bromm et al., 2018). However, with a correlation coefficient of 0.85 and an ϵ_{RMS} of 1.9 deg, the matching is still good.

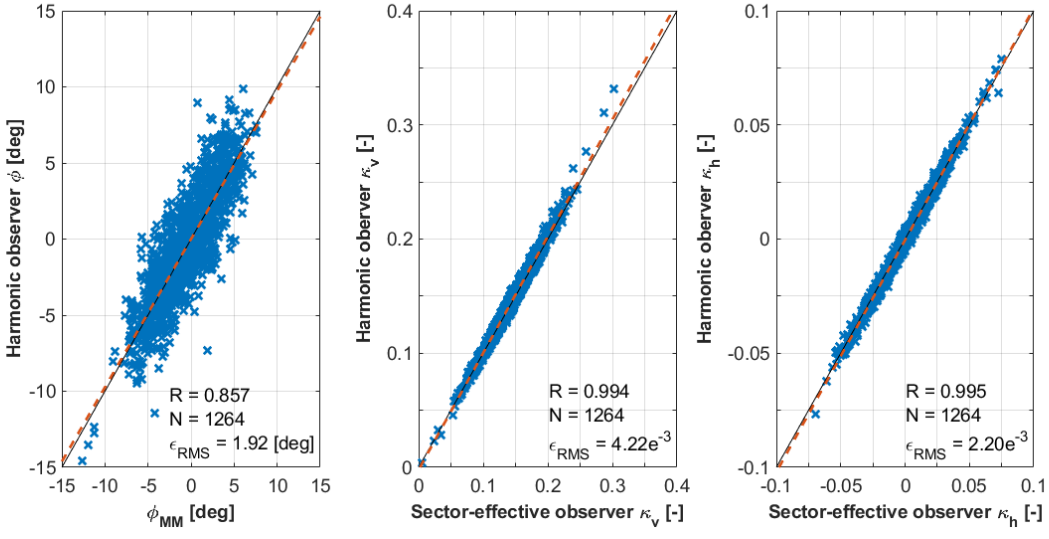

Figure 7. Correlation of 10-min averages between estimated parameters (y axis) and their reference quantities (x axis) for $V \geq 8$ m/s. From left to right: yaw misalignment angle, vertical linear shear, horizontal linear shear. Red dashed line: linear best fit; black dashed line: ideal match; R: Pearson's correlation coefficient; N: number of data points; ϵ_{RMS}: root mean square error.

It is very interesting to observe that, although the model was trained only with 10-min averages, it is still able to provide for time-resolved estimates of the parameters. To illustrate this fact, Fig. 8 reports a 10 Hz time history of the vertical shears from

https://doi.org/10.5194/wes-2020-83
Preprint. Discussion started: 9 July 2020

eawe european academy of wind energy
Open Access WIND ENERGY SCIENCE DISCUSSIONS

the validation sub-set. The figure corresponds to about two days of operation, during which the wind direction (bottom plot) was $\Gamma \in [145, 260]$ deg. Turbine and met-mast are roughly aligned for $\Gamma \in [177.5, 215]$ deg; WT1 is in the wake of WT2 for approximatively $\Gamma \in [120, 170]$ deg, the two directions being indicated in the plot with two horizontal dashed lines. The top plot of the figure shows the lower-half-rotor shears measured at the met-mast and by the sector-equivalent speeds. Although some discrepancies are present, the figure shows that the sector-effective observer is capable of following the main changes in shear captured by the met-mast. The main discrepancies can be found between 2PM of October 21 and about 4AM of October 22, when WT1 is in the wake of WT2 or in its close proximity. However, one should not forget that the two estimates correspond to two locations spaced 2.5D apart, and that the exact ground truth at the rotor disk —where the observers operate— is unknown. The central plot of the same figure shows the rotor-equivalent shear estimated by Eq. (8) based on rotor harmonics and its reference quantity obtained by the sector-equivalent speeds. The two vertical shears are in excellent agreement, even with respect to relatively fast fluctuations.

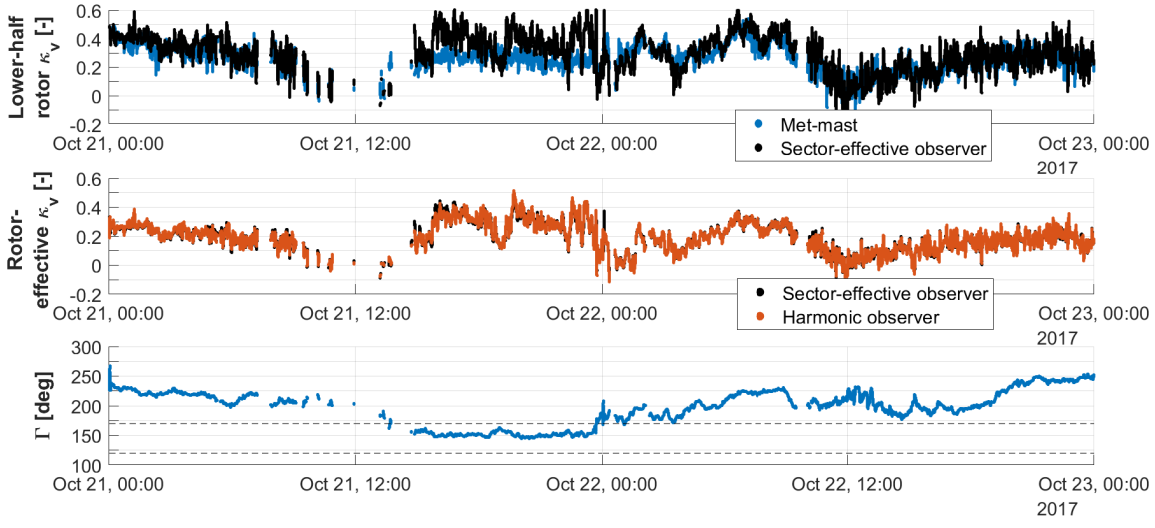

Figure 8. Time history of vertical shears at 10 Hz. From top to bottom: lower-half-rotor shear from the met-mast (blue) and the sector-effective observer (black); full-rotor-equivalent shear using Eq. (8) (red) and reference from the sector-effective observer (black); wind direction measured at the met-mast, with WT1 in the wake of WT2 between 120 and 170 deg (dashed horizontal lines).

To provide for a more complete statistical characterization of the observer performance, the 10-min data points were binned for the various relevant parameters. For each bin, the mean absolute error (MAE) between the estimated θ_{E} and reference θ_{R} wind parameter was computed as $\epsilon = 1/N \sum_i^N |\boldsymbol{\theta}_{\mathrm{R}_i} - \boldsymbol{\theta}_{\mathrm{E}_i}|$.

Figure 9 shows the MAE ϵ for yaw misalignment (top left), vertical and horizontal shear (top and bottom right, respectively), plotted as functions of binned wind speed, for various binned turbulence intensity (TI) levels. The number of available hours of data is reported in the bottom left histogram of the figure, to help determine the statistical significance of the results. Looking

https://doi.org/10.5194/wes-2020-83
Preprint. Discussion started: 9 July 2020

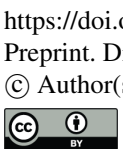

eawe european academy of wind energy
Open Access WIND ENERGY SCIENCE DISCUSSIONS

at the yaw angle results, it appears that the maximum error is about 3 deg and that accuracy tends to increase for higher wind speeds. Moreover, TI appears to play only a small effect on the results. The error in the vertical shear includes the error between the met-mast and the sector-effective observer of §2.3.2. Even in this case the error is small, and effects of TI are present but relatively mild. The figure also reports the horizontal shear, whose error —although very small— might not be very indicative, as no reference value was available from the met-mast for this quantity.

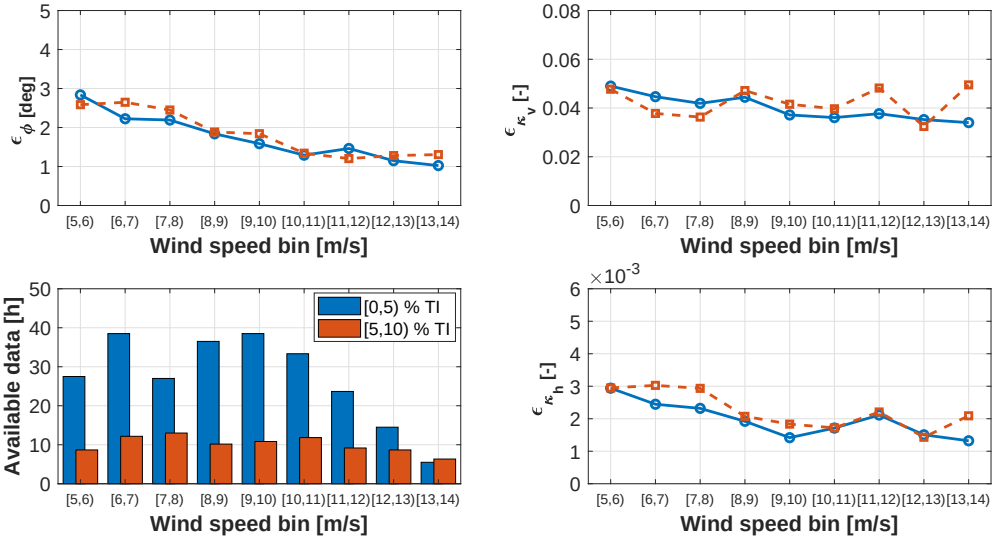

Figure 9. MAE ϵ vs. binned rotor-effective wind speed, for binned TI. Top left: yaw misalignment; top right: vertical shear; bottom right: horizontal shear; bottom left: hours of available data.

Figure 10 reports the results for varying binned air density. The plots show that the density correction of §2.2.1 is not perfect, probably because of an only approximate identification of the gravity term in Eq. (11).

Finally, Fig. 11 reports the results for varying wind direction. Looking at the vertical shear, the best results are obtained for wind directions between 170 and 210 deg, when turbine and met-mast are aligned, whereas the error increases significantly for other wind directions. When turbine and met-mast are not aligned, the two can be subjected to slightly different inflows, on account of orographic and vegetation-induced effects. This indicates once again that, as noted earlier on, the information provided by the reference met-mast cannot be regarded as an absolute ground truth. The yaw misalignment angle seems to be less influenced by these local effects, which might induce stronger local changes in shear than in direction at this particular site.

https://doi.org/10.5194/wes-2020-83
Preprint. Discussion started: 9 July 2020

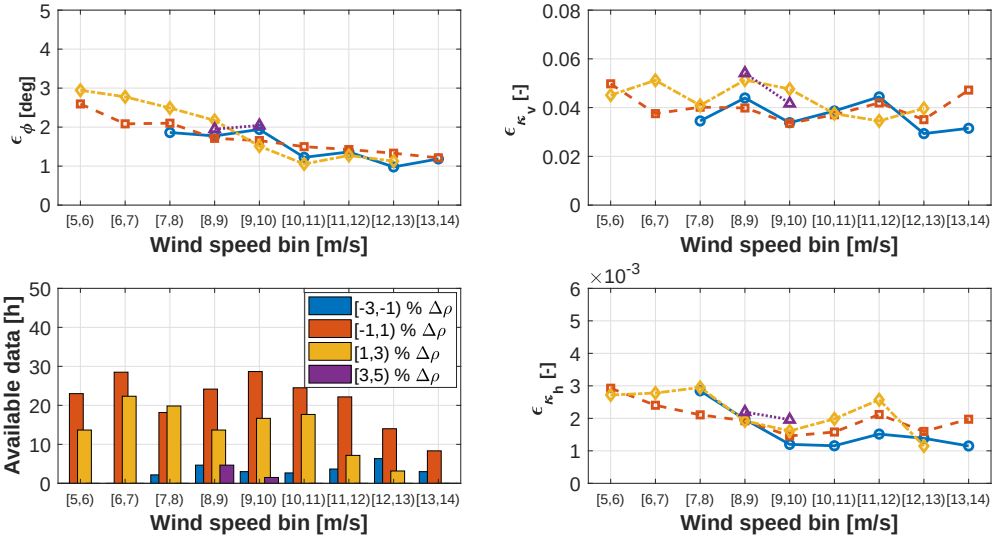

Figure 10. MAE ϵ vs. binned rotor-effective wind speed, for binned density change $\Delta\rho$ wrt. standard air. Top left: yaw misalignment; top right: vertical shear; bottom right: horizontal shear; bottom left: hours of available data.

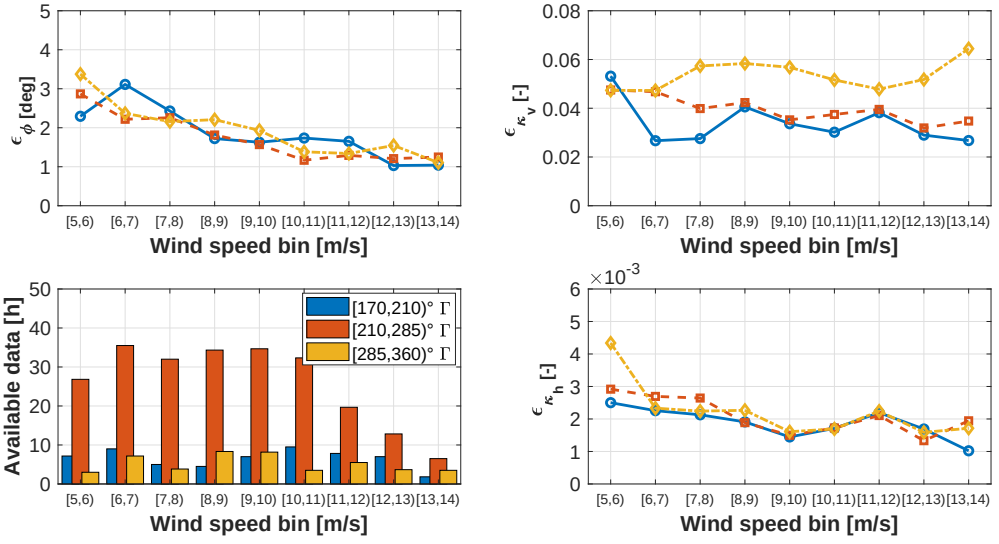

Figure 11. MAE ϵ vs. binned rotor-effective wind speed, for binned wind direction Γ. Top left: yaw misalignment; top right: vertical shear; bottom right: horizontal shear; bottom left: hours of available data.

https://doi.org/10.5194/wes-2020-83
Preprint. Discussion started: 9 July 2020

eawe european academy of wind energy
Open Access WIND ENERGY SCIENCE DISCUSSIONS

4 Conclusions

This paper has presented the application of a previously published harmonic-based wind sensing method to an experimental dataset. The setup at the test site is not complete enough to provide for a true field validation of the method. However, it is representative of a practical scenario where, by using a hub-tall certification met-mast, the method is trained for a given turbine model, before being deployed on assets of that same type at other production sites. After having explained the methodology and described the test site, the paper has also formulated a new method to extend the shear measured by a hub-tall mast to the tip of the rotor, in order to compute a full-rotor shear.

Based on the results analyzed herein, and notwithstanding the limits of the present dataset, the following conclusions can be drawn:

- There is a good correlation between met-mast and estimated lower-half rotor shears;
- There is an excellent correlation between the full-rotor shear extended above the mast and the one estimated by harmonic loads;
- Training with 10-min data improves the quality of the estimates with respect to the case where a much larger set of higher-sampling-frequency data points are used.
- Notwithstanding a training based on 10-min averages, the quality of the correlation between estimates and references does not only apply to 10-min quantities, but it also extends to time-resolved 10 Hz signals. In this sense, the observer seems capable of following relatively fast changes in shear. This might be useful for certain application scenarios, as for example the tracking of horizontal shears induced by wake interactions.
- There is a non-negligible effect of wind-mast-turbine non-exact alignment. In this sense, the actual quality of the correlation might be even better than what appears from the results shown here. This is in fact an intrinsic limit of field testing, where an exact ground truth is in general difficult if not impossible to obtain. Realistic simulations and wind tunnel studies as the ones reported in Bertelè et al. (2017, 2018, 2019) —where the ground truth is known— may help in this sense.
- Yaw misalignment is also estimated with reasonable quality, although the results here are less conclusive due to the fact that the met-mast reference is a point-wise measurement that might not fully represent rotor-effective conditions.
- There is only a modest effect of TI, which supports the hypothesis that 1P harmonics are mostly driven by “deterministic” wind characteristics and less affected by turbulent fluctuations.
- Notwithstanding the complicated effect of gravity on harmonic load components, its presence can be eliminated with enough accuracy to allow for a reasonably precise density correction.

A continuation of this work would greatly benefit from access to a more complete dataset, without the limits discussed above. Multiple, independent rotor-effective measurements of the inflow in very close proximity of the rotor disk would be

https://doi.org/10.5194/wes-2020-83
Preprint. Discussion started: 9 July 2020

necessary to establish an effective ground truth. This would allow for a better characterization of the accuracy of this method, and to study the effects induced by training with a standard hub-tall mast. A remaining open point is the demonstration that the method can indeed be trained on a turbine and, then, applied to another machine of that same model at another site; although this seems to be a very reasonable assumption, the evidence that this is indeed possible is lacking. Finally, it remains to be shown that the method does not need to be re-trained for an aging turbine. Here again, based also on the reassuring results already reported by Bottasso and Riboldi (2015), it is difficult to believe that 1P loads might change over time to the point of affecting the estimates, although a field proof of this assertion is clearly missing at this point in time.

Acknowledgements. The authors express their gratitude to Stefan Bockholt and Alexander Gerds of eno energy systems GmbH, who granted access to the measurement data and turbine model, and to Marijn van Dooren, Anantha Sekar and Martin Kühn of ForWind Oldenburg, who shared insight on the data. This work has been supported by the CompactWind II project (FKZ: 0325492G), which receives funding from the German Federal Ministry for Economic Affairs and Energy (BMWi).

Nomenclature

A	Rotor area
C_m	Cone coefficient
H	Height of the hub above ground
m	Blade bending moment
$\boldsymbol{m}$	Vector of moment harmonics
N	Number of available data points
q	Dynamic pressure
R	Rotor radius or Pearson's coefficient
$\boldsymbol{Q}$	Covariance matrix
V	Wind speed
V_h	Wind speed at hub height
V_S	Sector-effective wind speed
V_{TB}	Torque-balance rotor-effective wind speed
$\tilde{v}$	Non-dimensional tangential cross flow at hub height
$\tilde{w}$	Non-dimensional vertical cross flow at hub height
x, y, z	Hub-centered nacelle-attached axes
β	Pitch angle
Γ	Wind direction
ϵ	Mean absolute error
$\boldsymbol{\theta}$	Wind state vector

https://doi.org/10.5194/wes-2020-83
Preprint. Discussion started: 9 July 2020

eawe european academy of wind energy
Open Access WIND ENERGY SCIENCE DISCUSSIONS

κ_h	Horizontal shear
κ_v	Vertical shear
λ	Tip speed ratio
ρ	Air density
ϕ	Yaw misalignment angle
χ	Upflow angle
ψ	Azimuth angle
Ω	Rotor speed
$(\cdot)^T$	Transpose
$(\cdot)^{\mathrm{IP}}$	In-plane component
$(\cdot)^{\mathrm{OP}}$	Out-of-plane component
$(\cdot)_{\mathrm{1c}}$	1P cosine amplitude
$(\cdot)_{\mathrm{1s}}$	1P sine amplitude
$(\cdot)_{\mathrm{E}}$	Estimated quantity
$(\cdot)_{\mathrm{MM}}$	Met-mast measurement
$(\cdot)_{\mathrm{ref}}$	Reference quantity
$(\cdot)_{\mathrm{RMS}}$	Root mean square
1P	Once per revolution
MAE	Mean absolute error
Lidar	Light detection and ranging
LUT	Look-up table
RMS	Root mean square
SEWS	Sector-effective wind speed
Sodar	Sound detection and ranging
TI	Turbulence intensity
WT	Wind turbine

https://doi.org/10.5194/wes-2020-83
Preprint. Discussion started: 9 July 2020

eawe european academy of wind energy
Open Access WIND ENERGY SCIENCE DISCUSSIONS

References

Bertelè, M., Bottasso, C.L., Cacciola, S., Daher Adegas, F. and Delport, S.: Wind inflow observation from load harmonics, Wind Energ. Sci., 2, 615–640, doi:10.5194/wes-2-615-2017, 2017.

Bertelè, M., Bottasso, C.L., Cacciola, S.: Simultaneous estimation of wind shears and misalignments from rotor loads: formulation for IPC-controlled wind turbines, J. Phys. Conf. Ser., 1037 032007, doi:10.1088/1742-6596/1037/3/032007, 2018.

Bertelè, M., Bottasso, C.L. and Cacciola, S.: Wind inflow observation from load harmonics: wind tunnel validation of the rotationally symmetric formulation, Wind Energ. Sci., doi:10.5194/wes-2018-61, 2019.

Bertelè, M., Bottasso, C.L.: Initial results from the field testing of the "rotor as a sensor" concept, J. Phys. Conf. Ser., 1452 012074, doi:10.1088/1742-6596/1452/1/012074, 2020.

Bottasso, C.L. and Riboldi, C.E.D.: Estimation of wind misalignment and vertical shear from blade loads,Renew. Energ., 62, 293–302, doi:10.1016/j.renene.2013.07.021, 2014.

Bottasso, C.L. and Riboldi, C.E.D.: Validation of a wind misalignment observer using field test data, Renew. Energ., 74, 298–306, doi:10.1016/j.renene.2014.07.048, 2015.

Bottasso, C.L., Cacciola, S. and Schreiber, J.: Local wind speed estimation, with application to wake impingement detection, Renew. Energ., 116, 155–168, doi:10.1016/j.renene.2017.09.044, 2018.

Bottasso, C.L., Croce, A. and Riboldi, C.E.D.: Spatial estimation of wind states from the aeroelastic response of a wind turbine, The Science of Making Torque from Wind (TORQUE 2010), Heraklion, Crete, Greece, 28–30 June 2010.

Bromm, M., Rott, A., Beck, H., Vollmer, L., Steinfeld, G. and Kühn, M.: Field investigation on the influence of yaw misalignment on the propagation of wind turbine wakes, Wind Energy, 21, 1011–1028, doi:10.1002/we.2210, 2018.

Cacciola, S., Bertelè, M., Bottasso, C.L.: Simultaneous observation of wind shears and misalignments from rotor loads, J. Phys. Conf. Ser., 753(5),052002-1-8, doi:10.1088/1742-6596/753/5/052002, 2016.

Carswell, A.: Lidar measurements of the atmosphere, Canadian Journal of Physics, 6(2), 378–395, doi:10.1139/p83-049, 1983.

Coleman, R.P. and Feingold, A.M.: Theory of self-excited mechanical oscillations of helicopter rotors with hinged blades, Technical Report, NACA TN 1351, 1958.

Lang, S. and McKeogh, E.: LIDAR and SODAR Measurements of Wind Speed and Direction in Upland Terrain for Wind Energy Purposes, Remote Sensing, 3, 1871–1901, doi:10.3390/rs3091871, 2011.

International Electrotechnical Commission: DV IEC 61400-12-1, Technical Report, IEC, 2017.

Jonkman, J. and Jonkman, B.: FAST v7, https://nwtc.nrel.gov/FAST7, 2018.

Ma, X., Poulsen, N. and Bindner, H.: Estimation of Wind Speed in Connection to a Wind Turbine, Technical Report, Informatics and Mathematical Modelling, Technical University of Denmark, 1995.

Murphy, P., Lundquist, J. K., and Fleming, P.: How wind speed shear and directional veer affect the power production of a megawatt-scale operational wind turbine, doi:10.5194/wes-2019-86, 2019.

Schreiber, J., Cacciola, S., Campagnolo, F., Petrovic´, V., Mourembles, D., and Bottasso, C. L.: Wind shear estimation and wake detection by rotor loads — First wind tunnel verification, Journal of Physics: Conference Series, 753, 032 027, doi:10.1088/1742-6596/753/3/032027, 2016.

Schreiber, J., Bertelè, M., and Bottasso, C.L.: Field testing of a local wind inflow estimator and wake detector, Wind Energ. Sci. Disc., doi:10.5194/wes-2020-48, 2020.

https://doi.org/10.5194/wes-2020-83
Preprint. Discussion started: 9 July 2020

Simley, E. and Pao, L.Y.: Evaluation of a wind speed estimator for effective hub-height and shear components, Wind Energy, 19(1), 167–184, doi:10.1002/we.1817, 2016.

Soltani, M., Knudsen, T., Svenstrup, M., Wisniewski, R., Brath, P., Ortega, R. and Johnson, K.: Estimation of rotor effective wind speed: a comparison, IEEE Trans. Control Syst. Technol. 21 (4) 1155e1167, doi:10.1109/tcst.2013.2260751, 2013.

Van der Hooft, E. L. and Engelen, T.: Estimated wind speed feed forward control for wind turbine operation optimisation, European Wind Energy Conference & Exhibition (EWEC 2004), London, UK, 22–25 November 2004.

Vogt, S. and Thomas, P.: SODAR — A useful remote sounder to measure wind and turbulence, Journal of Wind Engineering and Industrial Aerodynamics, 54–55, 163–172, doi:10.1016/0167-6105(94)00039-G, 1995.